HHS Public Access

Author manuscript

J Immunol. Author manuscript; available in PMC 2016 March 01.

Published in final edited form as:

J Immunol. 2015 March 1; 194(5): 2219–2231. doi:10.4049/jimmunol.1402376.

Cryptococcus neoformans-induced macrophage lysosome damage crucially contributes to fungal virulence[1]

Michael J. Davis[*,†], **Alison J. Eastman**[*,‡], **Yafeng Qiu**[*,§,¶], **Brian Gregorka**[‖], **Thomas R. Kozel**[#], **John J. Osterholzer**[*,§], **Jeffrey L. Curtis**[*,‡,§], **Joel A. Swanson**[‖], and **Michal A. Olszewski**[*,‡,§,2]

[*]Division of Pulmonary & Critical Care Medicine, University of Michigan Health System, Ann Arbor, MI 48109

[†]MJD has subsequently moved to: National Institute for Allergy and Infectious disease Laboratory of Clinical Infectious disease, Bethesda, MD

[‡]Graduate Program in Immunology, University of Michigan, Ann Arbor, MI 48109

[§]VA Ann Arbor Healthcare System, Ann Arbor, MI 48105

[¶]Y. Qiu has subsequently moved to Shaghai Veterinary Research Institute, Chinese Agricultural Academy of Science, Shanghai 200241 China

[‖]Department of Microbiology & Immunology, University of Michigan Medical School, Ann Arbor, MI 48109

[#]Department of Microbiology & Immunology, University of Nevada School of Medicine, Reno, NV 89557

Abstract

Upon ingestion by macrophages, *Cryptococcus neoformans* (*Cn*) can survive and replicate intracellularly unless the macrophages become classically activated. The mechanism enabling intracellular replication is not fully understood; neither are the mechanisms which allow classical activation to counteract replication. *Cn*-induced lysosome damage was observed in infected murine bone marrow-derived macrophages, increased with time and required yeast viability. To demonstrate lysosome damage in the infected host, we developed a novel flow-cytometric method for measuring lysosome damage. Increased lysosome damage was found in *Cn*-containing lung cells compared to *Cn*–free cells. Among *Cn*-containing myeloid cells, recently recruited cells displayed lower damage than resident cells, consistent with the protective role of recruited macrophages. The magnitude of lysosome damage correlated with increased *Cn* replication. Experimental induction of lysosome damage increased *Cn* replication. Activation of macrophages with IFN-γ abolished macrophage lysosome damage and enabled increased killing of *Cn*. We

[1]This project was funded by VA merit (1I01BX000656-01A1; M.A.O.), NIH R01 grant GM101189 (J.A.S.) and NIH R01 AI014209 (T.R.K.). M.J.D. was supported by Multidisciplinary Training Program in Pulmonary Disease (PHS T32-HL07749-19).

[2]Address correspondence to: Dr. Michal Olszewski, Division of Pulmonary & Critical Care Medicine, University of Michigan Health System and VA Ann Arbor, Ann Arbor, MI 48105-5620, Tel: 734-845-5238, Fax: 734-845-3241, olszewsm@med.umich.edu.

Conflict of interest statement: The authors declare that they have no financial conflicts of interest in regards to the project being submitted in this manuscript.

conclude that induction of lysosome damage is an important *Cn* survival strategy and that classical activation of host macrophages counters replication by preventing damage. Thus, therapeutic strategies which decrease lysosomal damage, or increase resistance to such damage, could be valuable in treating cryptococcal infections.

Introduction

Cryptococcus neoformans (*Cn*) is an opportunistic fungal pathogen of global significance. *Cn* infection occurs with incidence of one million new cases each year (1) and is associated with a high level mortality (2). Especially in immune-compromised populations, uncontrolled fungal pneumonia is followed by highly lethal dissemination to the central nervous system (1–4).

Resident alveolar macrophages are among the first host cells to contact *Cn* and the pathogen is frequently found within lung macrophages (5). As the infection escalates, monocytes are recruited and mature into inflammatory “exudate” macrophages (6). Based on external signals, especially secreted cytokines, macrophages become classically or alternatively activated. Naïve and alternatively activated macrophages are insufficient to control *Cn* infection, allowing intracellular growth of the yeast (7–10). In contrast, classically activated macrophages can kill *Cn in vivo* (6, 8, 11, 12) and classically-activated exudate macrophages are a particularly important effector cell in this system (6). Classical macrophage activation and subsequent clearance of *Cn* requires the support of adaptive immunity (13–20).

Following ingestion by macrophages and other phagocytes, *Cn* organisms enter host lysosomes (21–26). Lysosomes are membrane-limited organelles, the contents of which are maintained at about pH 4.75 in macrophages by the vacuolar ATPase (27, 28), in contrast to the neutral pH of the surrounding cytosol. Lysosomes contain a variety of homeostatic and microbicidal hydrolases and numerous specialized microbicidal activities, including critical constituents of the phagocyte oxidase system, which catalyzes the production of microbicidal reactive oxygen species into the lysosomal lumen. *In vitro*, purified lysosomal components from dendritic cells are toxic to *Cn* (23, 26). In spite of these strong lysosomal defenses, naïve macrophages containing *Cn* become quickly overgrown by *Cn in vitro*. Also, individuals that succumb to *Cn* infection as well as *Cn*-sensitive murine strains do not display primary deficiencies in macrophage populations or intrinsic problems with lysosomes. Thus, delivery of *Cn* to macrophage phagolysosomal compartment is insufficient to control cryptococcal infection without strong classical activation of macrophages (13–20) suggesting that *Cn* possess some robust ability to counter the microbicidal properties of host lysosomes.

How *Cn* survive and replicate when faced with the toxic environment of the phagolysosome is unknown. One survival mechanism employed by other pathogens faced with a similar challenge, such as Candida, is to damage the lysosome phospholipid membrane (29). Although it is unknown if lysosome damage importantly contributes to intracellular virulence of *Cn* within macrophages, previous studies provided some evidence of *Cn*-associated effects on phagosomal membrane integrity and postulated phagolysosomal

damage (24, 30, 31). However, relative frequency and the extent of *Cn*-mediated phagolysosomal damage have not yet been quantitatively measured in *Cn*-infected live macrophage. Furthermore, it is unknown if such damage would be an important mechanism for intracellular survival of *Cn* within macrophages. We hypothesized that *Cn* actively damages host macrophage phagolysosomes to facilitate its intracellular growth within macrophages and that classical activation of macrophages limits *Cn*-mediated phagolysosome damage as a mechanism to inhibit *Cn* growth and to promote *Cn* killing by macrophages during protective immune responses.

Here we demonstrate that intracellular *Cn* causes progressive and substantial lysosome damage during growth within murine macrophages *in vitro* and *in vivo* and that IFN-γ-stimulation of macrophages limits damage, reduces *Cn* growth, and increases intralysosomal *Cn* killing. This study utilized recently developed live-cell microscopy techniques to provide quantitative and sensitive measurement of lysosome damage and a novel flow cytometric strategy to evaluate damage occurring in the lungs of *Cn*-infected animals. These data provide evidence that lysosome damage is a crucial mechanism employed by *Cn* to promote its intracellular virulence and that inducible lysosome renitence is an important mechanism that contributes to *Cn* control within activated macrophages.

Materials and Methods

Materials

We purchased the following tissue culture reagents from Life Technologies (Carlsbad, CA): RPMI 1640, Phenol Red-free RPMI 1640, Dulbecco's Modified Eagle Medium, fetal calf serum, GlutaMAX, sodium pyruvate, Non-essential amino acids, penicillin/ streptomycin, Hank's buffered saline solution (HBSS), nigericin, valinomycin, fluorescein dextran (average molecular weight 3,000 Daltons), Texas Red dextran (average molecular weight 3,000 Daltons) and SYTOX red. Recombinant IFN-γ, TNF-α and M-CSF were purchased from Peprotech, Inc (Rocky Hill, NJ). Recombinant IL-4 as well as APC-cy7 conjugated anti-CD11c (clone N418), perCP-cy5.5 conjugated anti-CD45 (clone 30F11) and PE-cy7 conjugated anti-Gr-1 (clone RB6-8C5) were from Biolegend (San Diego, CA). Sabouraud Dextrose broth and agarose were purchased from BD biosciences (San Jose, CA). Normal mouse serum was from Innovative Research (Novi, MI). Fluconazole was purchased from Sigma-Aldrich Corporation (St. Louis, MO). Uvitex-2B was purchased from Polyscience, Inc (Warrington, PA). Glass bottom culture dishes (catalog # P35G-1.5-14-C) were from Mat-tek Corporation (Ashland, MA). Dextran doubly-conjugated with fluorescein plus sulfarhodamine 101 (average molecular weight approximately 10,000 Daltons) was a custom product purchased from TdB Consultancy (Uppsala, Sweden).

Mice

BALB/C (Jackson Labs, Bar Harbor, ME) and C57BL/6 (Taconic Farms Inc, Hudson, NY) were housed at the Veterans Affairs Ann Arbor animal care facility, and were used at around 5–7 weeks of age.

Animal Ethics Statement

Animal care and use were performed in strict accordance with an animal use protocol reviewed and approved by the Veterans Affairs Institutional Animal Care and Use Committee (Permit Number 0512-025) in accordance with the Guide for the Care and Use of Laboratory Animals of the National Institutes of Health. All surgery was performed under ketamine and xylazine anesthesia and every effort was made to minimize suffering.

C. neoformans culture

Cryptococcus neoformans (*Cn*) strain H99 (ATCC 208821) was cultured as previously described (6, 12, 32). Briefly, cultures started from aliquots frozen in 10% glycerol were incubated at 37°C for four days in Sabouraud Dextrose broth. For use *in vitro* and *in vivo*, *Cn* were washed in sterile saline. For some experiments, *Cn* were heat-killed by boiling for 4 hours. For all *in vivo* infections and some *in vitro* infections, *Cn* were labeled with Uvitex-2B as in (33) in phosphate buffered saline (PBS) at 1×10^7 *Cn* per mL using 100 μg/mL Uvitex-2B.

Bone marrow derived macrophage culture

Macrophages were differentiated from bone marrow as previously described (32, 34–36). Briefly, marrow was flushed from the mouse long bones and dispersed into a single cell suspension. These cells were cultured for seven days in Dulbecco's Modified Eagle Medium supplemented with 20% fetal calf serum and 50 ng/mL recombinant M-CSF. Cultures were nourished with additional M-CSF-containing media on the third day of culture. All *in vitro* experiments were performed in RPMI containing 10% fetal calf serum and 5 ng/mL of M-CSF.

Loading macrophage lysosomes

For microscopy, suspended macrophages were plated onto coverslips placed in glass-bottomed culture dishes at 8×10^4 cells per coverslip. After allowing several hours for the cells to attach, the culture media was replaced with media containing 150 μg/mL Fdx. Following overnight incubation, cells were rinsed thoroughly with warmed HBSS and cultured in media without dye-dextran for at least three hours to insure that all internalized dye had trafficked into the macrophage lysosomes.

In vitro infection of macrophage

Saline-rinsed *Cn* were opsonized by 45 minute incubation with 10 μg/mL *Cn*-specific F12D2 IgG1 and 20% normal mouse serum. The F12D2 IgG1 is a subclass-switch variant of the original F12D2 IgG3. The production and properties of the mAB F12D2 have been described (37). *Cn* were then diluted in culture media to 0.05–0.1 MOI, such that macrophages started experiments with, at most, one *Cn* per macrophage. Cultured macrophages were infected by replacing culture media with *Cn*-containing media. Macrophages and *Cn* were co-cultured for one hour, then extracellular *Cn* were rinsed away using warm HBSS. Next, *Cn*-infected macrophages were incubated in RPMI culture media containing 20 μg/mL fluconazole to inhibit replication of any remaining extracellular *Cn*.

Microscopy

Measurement of lysosome damage was performed as previously described (34, 35). At indicated times following infection, coverslip-dishes were rinsed and culture media replaced with HBSS. Dishes were then mounted onto the heated stage of the microscope. The microscope used for all imaging save for the experiments involving experimental induction of damage was an Olympus (Center Valley, PA) IX70 inverted epi-fluorescence microscope using 100x oil immersion objective (numerical aperture 1.30) and equipped with a X-cite 120 metal halide light source for fluorescence (EXFO, Mississauga, ON, Canada), a temperature controlled stage and a CoolSNAP HQ2 monochrome camera (cooled CCD, 1392x1040, 14-bit).

To measure lysosome damage, we acquired three images: the first using a 436 nm excitation filter, another using a 492 nm excitation filter (in both cases using a 535 nm emission filter), and finally a phase contrast image. In some experiments, Uvitex-2B was measured using a 405 nm excitation filter and a 465 nm emission filter. All optical filters were from Chroma Technology Corporation (Bellows Falls, VT).

Image analysis

Image analysis was performed using Metamorph software as previously described (34, 35) (Molecular Devices, Downington, PA). Briefly, background signals were subtracted from all images and signal distortions from uneven illumination were corrected by dividing all acquired images by a normalized image acquired from a control sample with an even level of fluorophore. We determined intracellular pH based on the differential emission of fluorescein, which is largely pH-independent in the 436 nm excitation channel but highly pH-dependent on pH in the 492 nm excitation channel. Ratio images (492 nm signal/436 nm signal) were translated to pH maps based on microscope calibration. To calibrate the microscope, 492-nm/436-nm ratio images were acquired as above from macrophages identically labeled with Fdx in pH clamping buffer (130 mM KCl, 1mM $MgCL_2$, 15 mM HEPES, 15 mM MES). Clamping buffer contained 10 μM nigericin and 10 μM valinomycin which fix intracellular pH. Buffers were used at pH 9.0 to 4.0 using 0.5 pH unit increments. Average 492-nm/436-nm ratio values from cells at each pH were plotted and a four-variable sigmodial standard curve was constructed using Sigmaplot software (San Jose, CA) and pH maps were generated using this calibration data to convert 492 nm / 436 nm ratio values to pH. Regions showing pH greater than 5.5 indicated lysosome release and the percent of Fdx release was calculated by dividing the Fdx-fluorescence originating in regions depicting lysosome release by total cellular Fdx-fluorescence. We have previously shown pH 5.5 to be a valid empirical cutoff for these type of data (34, 35).

Enumeration of live versus dead *C. neoformans*

We observed differing morphological characteristics in *Cn* particles contained in Fdx loaded lysosomes depending on *Cn* viability. Live yeast excluded Fdx, thus the Fdx fluorescence appeared as annular halos on the perimeter of individual Fdx-dim yeast cells (Fig. 4A, upper row). In contrast, heat killed *Cn* absorbed lysosomal Fdx appearing as Fdx-bright filled bodies (Fig. 4A; lower). These properties were subsequently utilized to differentiate between viable and killed *Cn* experimentally based on fluorescence patterns in Fdx-containing

macrophage lysosomes. Using this difference in Fdx staining pattern, we enumerated live versus dead *Cn* inside imaged macrophages using Metamorph software. Although the vast majority of internalized yeast were live and excluded Fdx (Supplemental 1A), a detectable portion did not, consistent with a loss of *Cn* plasma membrane integrity and yeast death (Supplemental 1B & 1C). Semilunar or irregular morphologies, observed only among the dead yeast cells (Supplemental 1C), indicated lyosomal breakdown of *Cn*, consistent with previous reports in other cell types (5, 23, 26).

In vitro C. neoformans growth

These experiments were performed as previously published (32). To determine the ability of *Cn* to grow in macrophages, BMM were added to the wells of 24-well culture plates at 1×10^6 cells per well. Cells were stimulated overnight with cytokines (20 ng/mL IL-4, 20 ng/mL TNF-α and/or 100 ng/mL IFN-γ) as indicated. *Cn* cultures were opsonized and added at 2.5×10^4 *Cn* per well. After 24h, supernatants were removed and reserved then the intracellular fraction of *Cn* was liberated by lysing the macrophages in sterile water. We determined the number of *Cn* colony-forming units by serial dilution of samples plated on Sabouraud dextrose agar plates, which were counted after 48h. Data from supernatants and cellular fractions were summed during data analysis.

Experimental induction of lysosome damage

A second microscope was used for these experiments. This instrument was a Nikon TiE (Tokyo, Japan) inverted epi-fluorescence microscope using 40x (numerical aperture 0.95) and 4x (numerical aperture 0.20) air immersion objectives and a motorized stage. Fluorescence illumination was generated by a Lumencor Spectra X light engine (Beaverton, OR) and images acquired using a CoolSNAP HQ2 monochrome camera. Samples were maintained at 37 degrees Celsius using an OKO labs (Olivetti, Italy) stage incubator.

Our photo-induced damage protocol was based on previously published methods (34, 38). BMM (2×10^4) were spotted onto the center of Mat-tek coverslips in 50 μL of cell-containing RPMI. This resulted in a spot of macrophages attached to the coverslip approximately 4 mm in diameter. These cells were loaded with 150 μg/mL Fdx and 75 μg/mL Texas Red dextran, rinsed, chased and infected with Uvitex-2B-labeled H99 *Cn* as above. As imaging and photo exposure was conducted in medium, all medium used for these experiments was phenol red-free RPMI. Two hours post infection, excess *Cn* were rinsed away then the media replaced with fresh RMPI without serum. Next, coverslips were mounted onto the microscope stage. Using a 4x objective the cell covered area is located and exposed to bright orange/red light for 5 minutes using a 572/35 nm bandpass filter. The field size of the 4x objective allowed the vast majority of macrophages in the 4 mm spot to be simultaneously illuminated. Alternatively, control coverslips were incubated in the heated stage incubator for an identical time period without the photo exposure. Following exposure or mock exposure, cells were imaged using the 40x objective in a 7 × 7 grid pattern with 0.5 mm between each image; this pattern surveyed most of the cell covered area on the coverslip. Microscope control and imaging was controlled using Nikon- Elements Software. FCS was then added to each coverlip to 10% and cells incubated at 37 degrees Celsius with 5% CO_2. After 24 hours, colony forming unit count for *Cn* was determined as above. Image processing was

conducted using Metamorph software as above. Note, as these cells were imaged in bicarbonate containing medium their intracellular resting lysosomal pH was slightly higher than otherwise observed in control cells in other experiments, therefore the empirical cut-off for lysosome damage was raised from 5.5 to 5.75 for these experiments.

In vivo Infection of mice

Intratracheal administration of *Cn* was performed as previously described (6, 12, 39, 40) with some modifications for the administration of F/SR101dx. *Cn* cultures were rinsed in sterile saline, stained with Uvitex-2B and counted. These *Cn* were diluted into sterile saline containing 12 mg/mL sterile filtered F/SR101dx.

For the administration into mice, animals were anesthetized with ketamine and xylazine at 100 mg/kg and 6.8 mg/kg of bodyweight, respectively and immobilized on a surgical board. Under sterile technique, the trachea was exposed and inoculated with 1×10^6 *Cn* cells mixed with F/SR101dx or labeled macrophages in 40 μL of sterile saline using a 30-gauge needle. Control animals were administered F/SR101dx without *Cn*. The surgical wound was closed using cyanoacrylate adhesive and the mice were allowed to recover under thermal support. Mice were monitored daily for signs of distress until the completion of the experiment.

Bronchoalveolar lavage

Mice were sacrificed 48 hours post infection according to approved protocols. Lung airway cells were harvested by bronchoalveolar lavage as previously described (40). Briefly, the trachea was exposed and polyethylene tubing affixed using surgical twine. The lungs were lavaged 4 times with 1 mL per lavage with PBS containing 5 mM EDTA for a total volume of about 4 mL. Lavage cells were filtered through a nytex screen of 100 μM pore size and subsequently concentrated by centrifugation. Resuspended cells were then enumerated using a hemocytometer.

Flow cytometry

BAL samples were analyzed on a BD Biosciences LSRII flow cytometer system (San Jose, CA); instrument settings, including lasers and filters, have been described recently (41). Cells from bronchoalveolar lavage were analyzed by flow cytometry using two strategies. In the first strategy, designed to measure lysosome damage as quickly *ex vivo* as possible, cells were stained with SYTOX red for 15 minutes at room temperature in the dark then, immediately analyzed by flow cytometry. The second strategy aimed to identify myeloid cell sets, so samples were stained using the following antibodies; APC-cy7 conjugated anti-CD11c, perCP-cy5.5 conjugated anti-CD45 and PE-cy7 conjugated anti-Gr-1, then stained with SYTOX red and analyzed by flow cytometry. Compensation and spectral unmixing was applied through analysis of cells stained with antibodies against CD45 conjugated to the above fluorophores. Flow cytometric data was analyzed using FlowJo software (Tree Star, Inc, Ashland, OR).

Statistical analysis

Pairwise comparison depicted in figures 4C, 6B and 6C are unpaired Student t-tests between the indicated populations. All other bar graphs were analyzed by one-way ANOVA followed

by Student-Newman-Keuls method. ANOVA analysis showed significant differences between groups ($p<0.005$ for all experiments). Significant differences between individual groups by Student-Newman-Keuls method are as indicated in bar graph legends. Correlation data was analyzed by Pearson product-moment correlation coefficient analysis. All statistical analysis was conducted using SigmaPlot software (Systat Software Inc, Chicago, IL).

Results

Ingested *C. neoformans* replicates and induces lysosome damage in macrophages

Our first goal was to determine whether *Cn* induces significant lysosome damage. To measure the extent and kinetics of lysosome damage induced by *Cn*, we utilized a ratiometric fluorescence microscopic method developed by our group (34, 35). Cultured bone marrow-derived macrophages (BMM) were loaded overnight with FITC-dextran (Fdx) and then chased for several hours with fresh media, such that all Fdx was contained in lysosomes (27, 36, 42). The Fdx-loaded cells were infected with IgG-opsonized *Cn* at a low multiplicity of infection (MOI), such that macrophages started the experiment with one *Cn* per macrophage. Following one hour of infection, excess yeast were rinsed away and infected macrophages were imaged either immediately (1 hour post infection) or 24, 48 and 72 hours post-infection. Although *Cn*-phagosome-lysosome fusion was complete at one hour post-infection (Fig. 1A), there was no detectable lysosome damage at this time, as evidenced by containment of Fdx in exclusively acidic (red) compartments (Figs. 1A–C). In contrast, 24 hours later, significant lysosome damage was detectable in a subset of *Cn*-infected macrophages, indicated by Fdx which has been released into the neutral (cyan and blue) cytoplasm (Figs. 1A–C). Levels of lysosome damage increased over time as progressive increases in lysosomal Fdx released into the cytoplasm were observed 48 and 72 hours post-infection (Figs. 1A–C). No lysosome damage was observed in uninfected macrophages over the entire course of the experiment (Figs. 1A–C, **'No yeast')**.

The average number of intracellular yeast in each macrophage also increased over time, consistent with intracellular growth of *Cn* (Fig. 1D) and concurrent *Cn* replication and lysosome damage. While insufficient to overcome fungal growth, some fungicidal activity of macrophage was observed. A 15-fold increase of dye-incorporating dead yeast between 1h and 72h was observed (see supplemental figure 1 for demonstration of method). These killed *Cn* cells were a minor subset compared to the numbers live intracellular cryptococci, consistent with *Cn* replication prevailing over the active killing of the yeast inside macrophages (Fig. 1D).

To further assess the relationship between *Cn* growth and lysosomal damage we segregated macrophages 48 hours post infection into groups based on the number of *Cn* in each macrophage. Macrophages containing higher yeast burden displayed greater lysosome damage than did those with fewer yeast per macrophage (Fig. 1E). Collectively, these data demonstrate that ingested *Cn* induces lysosome damage in macrophages and that the damage is strongly linked to intracellular growth of *Cn*.

Alveolar phagocytes are subjected to *C. neoformans*-induced damage during pulmonary infection

To extend our *in vitro* observations to the natural course of cryptococcal infection *in vivo*, we used ratiometric flow cytometry to measure damage in phagocytes from the lungs of mice infected with *Cn* as described previously (6, 7, 12, 19, 20, 32). For these experiments, dextran conjugated to both pH sensitive FITC and pH insensitive sulforhodamine 101 (F/SR101dx) was administered to mice intratracheally, with or without Uvitex-2B-labeled *Cn* (Fig. 2Ai). This dye is taken up by lung cells and trafficked into lysosomes. The acidic environment of the lysosome depresses the FITC signal, resulting in a low FITC/SR101 ratio in cells with intact lysosomes. Subsequent damage releases the lysosomal F/SR101dx into the pH neutral cytosol increasing the fluorescence of FITC and thus raising the FITC/SR101 ratio (Fig 2Aii).

In uninfected mice receiving F/SR101dx, the majority of alveolar cells recovered by bronchoalveolar lavage (BAL) displayed high levels of SR101 fluorescence (Fig. 2B; **red box)** and low FITC/SR101 average ratios (Fig. 2C), indicating a low baseline level of phagolysosomal damage and that the cells were largely unperturbed by the cell isolation process. In mice which received both F/SR101dx and Uvitex-2B-stained *Cn*, we detected F/SR101dx+ cells (Fig. 2D, **red box)** as well as many F/SR101dx^{dim} cells. Among the F/SR101dx+ cells, many displayed sub-threshold Uvitex-2B fluorescence and thus did not contain *Cn*. These cells (Fig. 2E; **lower cell population)** displayed only background levels of phagolysosomal damage, similar to those from uninfected mice (Fig. 2C; **lower cell population)**. In contrast, cells with high Uvitex-2B fluorescence, indicating the cells contained intracellular *Cn* (Fig. 2E; **upper cell population),** showed higher average phagolysosomal damage (Fig. 2F) and increased percentages of phagolysosomal damage-positive cells (Fig. 2G), compared either to cells from uninfected mice or to the uninfected cells from infected mice. Thus, phagolysosomal damage occurs in *Cn*-infected cells *in vivo*.

Dextran-positive cells in the alveolar space at 48 hours post-infection are mostly alveolar macrophages

Alveolar macrophages are the predominant phagocyte population in the alveolar air spaces (6, 43, 44) and are thought to be the first cells to encounter *Cn* in the lungs. To establish that the F/SR101dx-containing cells at 48 h post infection were indeed alveolar macrophages, we analyzed cells recovered by BAL from F/SR101dx-treated, *Cn*-infected lungs by flow cytometry. The vast majority of CD11c+ BAL leukocytes contained F/SR101dx in both the uninfected mice (96.3±0.6%; mean ± SEM) (Fig. 3A) and *Cn*-infected mice (88.7±2.1%) (Fig. 3B). The converse was also true, in that virtually all of F/SR101dx-containing cells were CD11c+ in uninfected mice (90.5±1.8%) and infected mice (91.4±1.2%). The CD11c+, F/SR101dx+ cells were also CD45+ (Figs. 3C & D) and mainly GR-1^{dim}. Thus, F/SR101dx effectively labeled alveolar macrophages (CD11c+ CD45+ GR-1^{dim} cells) present in the mouse alveolar space and few other cells acquired significant levels of F/SR101dx.

Phagolysosomal damage occurs in alveolar and recently recruited macrophages

A small Gr-1+, CD11c+ and F/SR101dx+ triple-positive population (Fig. 3D, **top)** was observed in the lungs of infected mice (7.6±2.8% of CD11c+ F/SR101dx+ double-positive cells) while no such population (0.1±0.03%) was observed in the lungs of uninfected mice (Fig. 3C **top)**. Gr-1+ staining suggests that these were more recently recruited mononuclear phagocytes than the resident Gr-1^{dim} alveolar macrophage population. Phagolysosomal damage was observed in the *Cn*-containing cells from both the Gr-1+ (Figs. 3F and compare conditions "2" and "3" in H & I) and Gr-1^{dim} cells (Figs. 3G and conditions "4" and "5" in H & I). Interestingly, the phagolysosomal damage observed in the Gr-1+ population was less than that observed in the Gr-1^{dim} population (Figs 3H & I; **compare conditions "2" and "4")**. Thus, significant *Cn*-induced phagolysosomal damage was observed in both resident and infiltrating mononuclear phagocytes if they had ingested *Cn*.

Lysosome damage requires cryptococcal viability

In order to investigate the mechanisms underlying *Cn*-mediated lysosome damage we focused on BMM as an *in vitro* model of lung macrophages. Our next goal was to determine whether *Cn*-induced lysosome damage requires *Cn* viability. To address this, macrophages were administered IgG-opsonized live *Cn* or IgG-opsonized heat-killed *Cn*. At 48 hours post-infection, live *Cn* extensively damaged lysosomes whereas heat-killed *Cn* triggered only minimal release of Fdx (Fig. 4A & B). Because, unlike the heat-killed *Cn*, live yeast grew over the course of this experiment, we compared matching subsets of macrophages containing similar number of live versus heat-killed *Cn*. The lysosome damage was profoundly reduced in macrophages containing 4–7 of heat-killed *Cn* compared to those with an equivalent number of live yeast (Fig. 4C). These data indicated that live *Cn* is a much stronger inducer of lysosome damage than the killed organism and an active *Cn* process is required for the induction of lysosome damage.

Macrophage lysosome damage correlates with cryptococcal growth

Our data strongly suggest that *Cn* growth and lysosome damage are linked (Figs 1–4) implying that lysosome damage benefits *Cn*. To explore this hypothesis, *Cn* was labeled with Uvitex-2B (33, 45, 46), then used to infect Fdx-loaded macrophages. Before yeast replication, Uvitex-2B staining was bright (Fig. 5A; **red arrowheads)**. *Cn* replication diluted the dye, yielding dimly-stained, daughter cells (Fig. 5B; **yellow arrows)**, which could be readily enumerated separately from the brightly stained undivided yeast (Fig. 5B; **red arrowheads**). These properties were used to quantify replicative and non- replicative yeast. After 48h of infection, there were statistically significant correlations between the level of lysosome damage and numbers of divided (Uvitex-2B dim) *Cn* per macrophage (Fig. 5C; **$p<0.001$)** and the numbers of *Cn* that had both divided and remained viable (Fig. 5D; **$p<0.001$)**. These correlations indicate that macrophages showing more lysosome damage were more permissive of *Cn* growth and those that displayed less lysosome damage were better in controlling *Cn* growth, further supporting the notion that lysosome damage is a mechanism by which *Cn* promotes its intracellular survival and replication.

Experimentally-induced lysosome damage enhances cryptococcal growth

To test whether lysosome damage directly contributes to intracellular replication of *Cn* rather than simply accompanies *Cn* intracellular growth, we experimentally increased lysosome damage and assayed the effect of this damage on *Cn* replication. We utilized an established photo-damage protocol (34, 38) in which macrophage lysosomes were loaded with Texas Red-dextran, as a photosensitizer along with Fdx and subsequently the macrophages infected with Uvitex-2B-labeled *Cn*. To experimentally induce *Cn*-independent lysosome damage, the cells were then exposed to intense orange/red light, while control (mock exposed) cells were incubated on the microscope stage without light for a similar time period. The photo exposure-induced high levels of lysosome damage in most of the exposed cells, while the mock exposed cells remained at baseline levels of lysosome damage (Fig. 6A). In fact, the infected mock exposed cells displayed near baseline level of lysosome damage, while the infected photo exposed cells showed significantly increase release of lysosomal contents (Fig. 6B). Importantly, there was increased *Cn* replication in the photo exposed macrophages compared to the mock exposed macrophages (Fig. 6C) providing direct evidence that lysosome damage benefits *Cn* and increases the replication of the yeast.

Stimulation with IFN-γ induces lysosomal renitence which protects macrophages from *C. neoformans*-induced lysosomal damage

Classical activation of macrophages limits lysosome damage induced by bacterial pathogens and non-infectious particles via a mechanism termed inducible lysosome renitence (34). The major factor driving classical activation of macrophages, INF-γ, has been shown to be a key factor in reducing *Cn* growth by macrophages *in vitro* (32) and in limiting cryptococcosis *in vivo* (8, 11, 12, 40). To determine whether IFN-γ-induced lysosome renitence opposes *Cn*-mediated lysosome damage, macrophages were stimulated overnight either without cytokine or with IL-4, TNF-α, IFN-γ, or IFN-γ plus TNF-α; these treated macrophages were then infected with *Cn* and assessed for lysosome damage, *Cn* growth and killing of *Cn* at 24h post-infection. Once again, *Cn* infection induced high levels of lysosome damage in unstimulated macrophages (Figs. 7A & B). Somewhat unexpectedly, lysosomal damage was partially reduced by stimulation with IL-4, but not by TNF-α (Figs. 7A & B). In contrast, stimulation with IFN-γ almost entirely eliminated lysosome damage (Figs. 7A & B). Furthermore, the reduction of lysosome damage by IFN-γ was significant regardless of whether comparisons involved all imaged macrophages (Percent Fdx release for unstimulated macrophages: 21.48±3.51 vs. IFN-γ-stimulated macrophages: 0.97±0.16; $p<0.001$ Student-Newman-Keuls) or only macrophages containing similar numbers (3–6 yeast per macrophage) of *Cn* (Fig. 7B). This suggests that IFN-γ stimulation inhibited *Cn*-induced lysosome damage independent of any IFN-γ-effects on *Cn* growth rate. Addition of TNF-α did not interfere with the IFN-γ-dependent reduction in *Cn*-mediated lysosome damage, as cells stimulated with both cytokines displayed very low levels of damage (Figs. 7A & B). IFN-γ stimulation of macrophages also reduced *Cn*-induced lysosome damage 48h post infection (Fig. 7F).

Stimulatory conditions which prevented lysosome damage reduced *C. neoformans* proliferation in macrophages

As lysosome damage increased *Cn* replication (Fig. 6) and was prevented by classical macrophage activation (Figs. 7A & B), we next asked whether limitation of *Cn* to macrophage lysosomes is a mechanism for constraining *Cn* growth. Accordingly, we enumerated microbial growth in macrophages stimulated with the various cytokines. Stimulation with IL-4 or TNF-a, which allowed significant lysosome damage (Fig. 7B), did not reduce microbial replication (Figs. 7C & E). In contrast, stimulation with IFN-γ, which limited lysosome damage (Fig. 7B), significantly reduced microbial replication (Figs. 7C & E). The IFN-γ-dependent reduction in *Cn* growth was also evident in experiments utilizing macrophages infected with Uvitex-2B stained *Cn,* in which both *Cn* division and the average number of divided *Cn* per macrophage were reduced by IFN-γ stimulation (Fig. 7G–I).

Consistent with these data, IFN-γ significantly increased macrophage killing of *Cn,* while IL-4 and TNF-α alone did not (Fig. 7D). Interestingly, dual stimulation with IFN-γ and TNF-α further reduced microbial growth beyond IFN-γ alone (Figs. 7C & E) and further increased fungal killing by macrophages (Fig. 7D). Collectively, these data indicate that IFN-γ activated macrophages prevent lysosome damage and thereby enable more efficient containment and killing of the microbes.

Discussion

We provide the first quantitative evidence that *Cn* induces lysosome damage in live macrophages. In addition, we demonstrate *bona fide* macrophage lysosome damage in the infected lung macrophage populations during early murine pulmonary cryptococcosis, a period of infection exhibiting rapid expansion of *Cn*. This damage requires viable *Cn* and its magnitude increases over time and with fungal growth in the macrophage (Fig. 8A). Our data demonstrate for the first time that lysosome damage contributes to the enhanced survival and intracellular growth of *Cn* (Fig. 8B). Combined these findings imply that initiation of damage to the phagolysomal membrane by viable *Cn* promotes the microbe's intracellular growth, which may, in turn, result in more extensive damage. The outcome of this vicious cycle is cumulative lysosome damage, extremely inefficient killing of *Cn* and robust *Cn* replication. We also show that IFN-γ stimulation can disrupt damage induction by *Cn* and that when *Cn* is contained within an undamaged lysosome by IFN-γ-induced lysosomal renitence, the cycle of intracellular *Cn* growth and progressive damage is disrupted (Fig. 8C). Collectively, these novel results identify lysosomal damage as an important mechanism of intracellular cryptococcal virulence, and demonstrate that prevention of that damage by IFN-γ-induced lysosomal renitence is required for maximal fungicidal activity by the macrophage.

Although there was some previous evidence of phagosomal disruption during *in vitro* cryptococcal infection of macrophage (30), the data presented here are the first to quantitatively measure *Cn*-mediated lysosome disruption *in vitro* and *in vivo* and to define damage as a live-pathogen induced, progressive biological process. It is unknown whether the observed *Cn*-mediated release of lysosomal contents is the result of exit of *Cn* from the macrophage endocytic compartment (similar to *Listeria monocytogenes*) or *Cn*-residence

inside a permeabilized but nevertheless existent membrane compartment (similar to *M. tuberculosis*). Although further research is required to determine the frequency of these two outcomes there is little evidence from previous electron microscopy studies for full *Cn*-escape from lysosomal membranes and residence in cytosol (5, 30). Collectively, our data show that lysosome damage rapidly develops in *Cn* infected macrophages both *in vitro* and *in vivo* and that it is associated with increased fungal growth and diminished killing by macrophages. To our knowledge this is the first evidence linking lysosome damage with cryptococcal intracellular growth.

We recently defined inducible lysosome renitence as a novel activity induced by several factors, including IFN-γ, which opposes lysosome damage induced by silica particles, photo exposure and *Listeria monocytogenes* (34). The data presented here show that IFN-γ-induced lysosomal renitence functioned to reduce *Cn*-induced lysosome damage which corresponded to a reduction in microbial growth and an increase in fungicidal activity (Fig. 7). Thus, induced lysosome renitence is a critical countermeasure for lysosome damage induced by fungi and an important mechanism by which the fungicidal activity of macrophages is potentiated by IFN-γ.

Our data show that increased lysosome damage results in enhanced cryptococcal growth and IFN-γ stimulation reduces lysosome damage and cryptococcal growth. This presents the dilemma of whether IFN-γ stimulation reduces *Cn*-mediated lysosome damage first which in turn causes a reduction in *Cn* growth (Fig. 8C), or whether IFN-γ stimulation reduces *Cn* growth independent of lysosomal integrity which then results in decreased lysosome damage (Fig. 8D). Although, we cannot definitively solve this causality dilemma, our previous work showed that IFN-γ stimulation reduces lysosome damage in non-microbial models where replication does not occur (34). Thus, it is likely that IFN-γ stimulation reduces lysosome damage independent of mere inhibition of *Cn* growth. This conclusion is re-enforced by figure 7B where lysosome damage was reduced by IFN-γ stimulation even when populations displaying equal levels of fungal growth were compared. Additionally, macrophage stimulation with TNF-α alone induces microbicidal effects against other microbes (47, 48), but did not result in induced lysosome renitence nor improved *Cn*-inhibition (Fig 5). However, when combined with IFN-γ-induced lysosome renitence, TNF-α considerably improved fungal killing. Taken together, we infer that the IFN-γ-dependent reduction in *Cn* growth and increase in *Cn* killing are crucially dependent on restriction of the microbe within the lysosomal compartment and are thus dependent on inducible lysosome renitence.

While *Cn*-induced lysosome damage and *Cn*-exocytosis (49, 50) both involve evasion of macrophage lysosomes we view these as biologically distinct mechanisms. Several published reports have hinted that phagosomal disruption is preferentially followed by *Cn*-exocytosis. First, drugs which increased phagosomal pH also increased *Cn*-exocytosis (33). Exocytosis was preceded by release of a dye-dextran from the *Cn*-containing phagosome (31). However in that work, there was no indication that the phagosomal dye was released into the cytosol as opposed to extracellular space. IFN-γ does not alter the frequency of cryptococcal expulsion (10), however, IFN- γ limited lysosome damage and preserved lysosomal pH (Fig. 7). Finally, the majority of exocytosis occurs during the first few hours

of macrophage infection, albeit tested at higher MOI (51) which is in contrast to the observed kinetics of phagolysosome damage where maximal damage occurred several days post infection (Fig. 1). Collectively, these data overwhelmingly support that *Cn*-exocytosis and *Cn*-mediated lysosome damage are chronologically and biologically independent.

The data presented here show that *Cn*–induced phagolysosome damage significantly enhances *Cn* virulence. In contrast, the effects of *Cn*-mediated phagolysosome damage on host macrophages as well as the *Cn*-processes underlying the induction of lysosomal damage both remain unknown. In (Coelho et al, Journal of Immunology; joint submission) the authors show that intracellular *Cn*-infection of macrophages results in macrophage programed cell death. These combined data sets open the possibility that *Cn*-induced phagolysosome damage may enhance programmed cell death in macrophages. Intriguingly, lysosome damage induced by ground silica has been shown to induce inflammasome activation and pyroptosis in activated macrophages (35, 52) consistent with the observed activation of caspase-1 in cells infected with fungal pathogens (53–56). Lysosome damage can also have a role in apoptosis as released lysosomal cathepsins can cleave apoptosis proteins to initiate programed cell death in cultured fibroblasts (57–65). While *Cn*-induced lysosome damage may trigger programed cell death, it is also possible that *Cn*-induced programed cell death induces or enhances lysosome damage. Reactive oxygen species from depolarized mitochondria can damage lysosomes (66). The activation of Bax and Bim can also lead to lysosomal destabilization (67–70). Thus, the *Cn*-mediated cell death observed in (Coelho et al, Journal of Immunology; joint submission) could be downstream, upstream or co-induced with *Cn*-mediated lysosome damage underscoring the need for future studies.

The effector cell population for *Cn* clearance *in vivo* has recently been defined by our group as fungicidal exudate macrophages (6). Significantly less lysosome damage was observed in the exudate macrophages than in resident alveolar macrophages on an individual cell basis (Fig. 3). Since, lysosome damage supports *Cn* growth (Figs. 5&6) and inversely correlates with fungal killing (Figs. 5&7), these data suggest that improved resistance to lysosome damage contributes to the proficiency of exudate macrophages as anti-fungal effector cells. Exudate macrophages were more prone to classical activation than alveolar macrophages (6, 71). Overall, these data provide new insight into possible mechanisms enabling exudate macrophages to contribute to anticryptococcal immunity.

In summary, our data provide the first complete evidence of a fungal pathogen utilizing lysosome damage as a virulence mechanism to overcome host defenses and to promote fungal persistence. It is also the first demonstration of lysosomal damage triggered by a pathogen *in vivo*. We further show that the host adaptive immune response counteracts this through IFN-γ mediated lysosomal renitence, especially within newly recruited exudate macrophages. The presence or absence of inducible lysosome renitence, which depends on the availability of extrinsic cytokines, expands our mechanistic understanding of cryptococcal opportunism in the context of macrophage-pathogen interaction. While further research is required, our data strongly imply that resistance to lysosome damage is a major mechanism that enables classically activated macrophages to combat infection by *Cn* and other invasive fungi. Thus, therapeutic strategies that oppose *Cn*'s ability to damage lysosomes or which bolster macrophage defenses against phagolysosomal damage, might

effectively compliment fungicidal agents in the treatment of cryptococcosis and possibly other invasive fungal infections in immunocompromised patients.

Supplementary Material

Refer to Web version on PubMed Central for supplementary material.

Acknowledgments

We thank Dr. Gary Huffnagle, University of Michigan and Dr. Robin May, University of Birmingham, UK for their helpful advice with data interpretation and Antoni Malachowski, Joudeh Freij, Jacob Carolan, Zachary Hadd, Woo Sung Cho, Ricky Pad and Nicole Potchen for their technical assistance in various parts of this study. We appreciate the support of Undergraduate Research Opportunity Program at the University of Michigan.

Abbreviations used in this article

Cn	Cryptococcus neoformans
BMM	Bone marrow-derived macrophage
Fdx	Fluorescein (FITC)-dextran
MOI	Multiplicity of infection
F/SR101dx	FITC and sulforhodamine 101 double labeled dextran

References

1. Park BJ, Wannemuehler KA, Marston BJ, Govender N, Pappas PG, Chiller TM. Estimation of the current global burden of cryptococcal meningitis among persons living with HIV/AIDS. AIDS. 2009; 23:525–530. [PubMed: 19182676]
2. Chuck SL, Sande MA. Infections with Cryptococcus neoformans in the acquired immunodeficiency syndrome. N Engl J Med. 1989; 321:794–799. [PubMed: 2671735]
3. Olszewski MA, Zhang Y, Huffnagle GB. Mechanisms of cryptococcal virulence and persistence. Future Microbiol. 2010; 5:1269–1288. [PubMed: 20722603]
4. Baddley JW, Perfect JR, Oster RA, Larsen RA, Pankey GA, Henderson H, Haas DW, Kauffman CA, Patel R, Zaas AK, Pappas PG. Pulmonary cryptococcosis in patients without HIV infection: factors associated with disseminated disease. Eur J Clin Microbiol Infect Dis. 2008; 27:937–943. [PubMed: 18449582]
5. Feldmesser M, Kress Y, Novikoff P, Casadevall A. Cryptococcus neoformans is a facultative intracellular pathogen in murine pulmonary infection. Infect Immun. 2000; 68:4225–4237. [PubMed: 10858240]
6. Osterholzer JJ, Chen GH, Olszewski MA, Zhang YM, Curtis JL, Huffnagle GB, Toews GB. Chemokine receptor 2-mediated accumulation of fungicidal exudate macrophages in mice that clear cryptococcal lung infection. Am J Pathol. 2011; 178:198–211. [PubMed: 21224057]
7. Osterholzer JJ, Surana R, Milam JE, Montano GT, Chen GH, Sonstein J, Curtis JL, Huffnagle GB, Toews GB, Olszewski MA. Cryptococcal urease promotes the accumulation of immature dendritic cells and a non-protective T2 immune response within the lung. Am J Pathol. 2009; 174:932–943. [PubMed: 19218345]
8. Arora S, Hernandez Y, Erb-Downward JR, McDonald RA, Toews GB, Huffnagle GB. Role of IFN-gamma in regulating T2 immunity and the development of alternatively activated macrophages during allergic bronchopulmonary mycosis. J Immunol. 2005; 174:6346–6356. [PubMed: 15879135]
9. Muller U, Stenzel W, Kohler G, Werner C, Polte T, Hansen G, Schutze N, Straubinger RK, Blessing M, McKenzie AN, Brombacher F, Alber G. IL-13 induces disease-promoting type 2 cytokines,

alternatively activated macrophages and allergic inflammation during pulmonary infection of mice with Cryptococcus neoformans. J Immunol. 2007; 179:5367–5377. [PubMed: 17911623]

10. Voelz K, Lammas DA, May RC. Cytokine signaling regulates the outcome of intracellular macrophage parasitism by Cryptococcus neoformans. Infect Immun. 2009; 77:3450–3457. [PubMed: 19487474]
11. Hardison SE, Ravi S, Wozniak KL, Young ML, Olszewski MA, Wormley FL Jr. Pulmonary infection with an interferon-gamma-producing Cryptococcus neoformans strain results in classical macrophage activation and protection. Am J Pathol. 2010; 176:774–785. [PubMed: 20056835]
12. Zhang Y, Wang F, Tompkins KC, McNamara A, Jain AV, Moore BB, Toews GB, Huffnagle GB, Olszewski MA. Robust Th1 and Th17 immunity supports pulmonary clearance but cannot prevent systemic dissemination of highly virulent Cryptococcus neoformans H99. Am J Pathol. 2009; 175:2489–2500. [PubMed: 19893050]
13. Syme RM, Bruno TF, Kozel TR, Mody CH. The capsule of Cryptococcus neoformans reduces T-lymphocyte proliferation by reducing phagocytosis, which can be restored with anticapsular antibody. Infect Immun. 1999; 67:4620–4627. [PubMed: 10456908]
14. Syme RM, Spurrell JC, Amankwah EK, Green FH, Mody CH. Primary dendritic cells phagocytose Cryptococcus neoformans via mannose receptors and Fcgamma receptor II for presentation to T lymphocytes. Infect Immun. 2002; 70:5972–5981. [PubMed: 12379672]
15. Syme RM, Spurrell JC, Ma LL, Green FH, Mody CH. Phagocytosis and protein processing are required for presentation of Cryptococcus neoformans mitogen to T lymphocytes. Infect Immun. 2000; 68:6147–6153. [PubMed: 11035718]
16. Arora S, McDonald RA, Toews GB, Huffnagle GB. Effect of a CD4-depleting antibody on the development of Cryptococcus neoformans-induced allergic bronchopulmonary mycosis in mice. Infect Immun. 2006; 74:4339–4348. [PubMed: 16790808]
17. Lindell DM, Moore TA, McDonald RA, Toews GB, Huffnagle GB. Generation of antifungal effector CD8+ T cells in the absence of CD4+ T cells during Cryptococcus neoformans infection. J Immunol. 2005; 174:7920–7928. [PubMed: 15944298]
18. Lindell DM, Moore TA, McDonald RA, Toews GB, Huffnagle GB. Distinct compartmentalization of CD4+ T-cell effector function versus proliferative capacity during pulmonary cryptococcosis. Am J Pathol. 2006; 168:847–855. [PubMed: 16507900]
19. Huffnagle GB, Lipscomb MF, Lovchik JA, Hoag KA, Street NE. The role of CD4+ and CD8+ T cells in the protective inflammatory response to a pulmonary cryptococcal infection. J Leukoc Biol. 1994; 55:35–42. [PubMed: 7904293]
20. Huffnagle GB, Yates JL, Lipscomb MF. Immunity to a pulmonary Cryptococcus neoformans infection requires both CD4+ and CD8+ T cells. J Exp Med. 1991; 173:793–800. [PubMed: 1672543]
21. Artavanis-Tsakonas K, Kasperkovitz PV, Papa E, Cardenas ML, Khan NS, Van der Veen AG, Ploegh HL, Vyas JM. The tetraspanin CD82 is specifically recruited to fungal and bacterial phagosomes prior to acidification. Infect Immun. 2011; 79:1098–1106. [PubMed: 21149584]
22. Artavanis-Tsakonas K, Love JC, Ploegh HL, Vyas JM. Recruitment of CD63 to Cryptococcus neoformans phagosomes requires acidification. Proc Natl Acad Sci U S A. 2006; 103:15945–15950. [PubMed: 17043215]
23. Hole CR, Bui H, Wormley FL Jr, Wozniak KL. Mechanisms of dendritic cell lysosomal killing of Cryptococcus. Sci Rep. 2012; 2:739. [PubMed: 23074646]
24. Levitz SM, Nong SH, Seetoo KF, Harrison TS, Speizer RA, Simons ER. Cryptococcus neoformans resides in an acidic phagolysosome of human macrophages. Infect Immun. 1999; 67:885–890. [PubMed: 9916104]
25. Weber SM, Levitz SM. Chloroquine antagonizes the proinflammatory cytokine response to opportunistic fungi by alkalizing the fungal phagolysosome. J Infect Dis. 2001; 183:935–942. [PubMed: 11237811]
26. Wozniak KL, Levitz SM. Cryptococcus neoformans enters the endolysosomal pathway of dendritic cells and is killed by lysosomal components. Infect Immun. 2008; 76:4764–4771. [PubMed: 18678670]

27. Christensen KA, Myers JT, Swanson JA. pH-dependent regulation of lysosomal calcium in macrophages. J Cell Sci. 2002; 115:599–607. [PubMed: 11861766]
28. Kinchen JM, Ravichandran KS. Phagosome maturation: going through the acid test. Nat Rev Mol Cell Biol. 2008; 9:781–795. [PubMed: 18813294]
29. El-Kirat-Chatel S, Dufrene YF. Nanoscale imaging of the Candida-macrophage interaction using correlated fluorescence-atomic force microscopy. ACS Nano. 2012; 6:10792–10799. [PubMed: 23146149]
30. Tucker SC, Casadevall A. Replication of Cryptococcus neoformans in macrophages is accompanied by phagosomal permeabilization and accumulation of vesicles containing polysaccharide in the cytoplasm. Proc Natl Acad Sci U S A. 2002; 99:3165–3170. [PubMed: 11880650]
31. Johnston SA, May RC. The human fungal pathogen Cryptococcus neoformans escapes macrophages by a phagosome emptying mechanism that is inhibited by Arp2/3 complex-mediated actin polymerisation. PLoS Pathog. 2010; 6:e1001041. [PubMed: 20714349]
32. Davis MJ, Tsang TM, Qiu Y, Dayrit JK, Freij JB, Huffnagle GB, Olszewski MA. Macrophage M1/M2 polarization dynamically adapts to changes in cytokine microenvironments in Cryptococcus neoformans infection. MBio. 2013; 4:e00264–00213. [PubMed: 23781069]
33. Nicola AM, Robertson EJ, Albuquerque P, da Derengowski LS, Casadevall A. Nonlytic exocytosis of Cryptococcus neoformans from macrophages occurs in vivo and is influenced by phagosomal pH. MBio. 2011:2.
34. Davis MJ, Gregorka B, Gestwicki JE, Swanson JA. Inducible renitence limits Listeria monocytogenes escape from vacuoles in macrophages. J Immunol. 2012; 189:4488–4495. [PubMed: 23002437]
35. Davis MJ, Swanson JA. Technical advance: Caspase-1 activation and IL-1beta release correlate with the degree of lysosome damage, as illustrated by a novel imaging method to quantify phagolysosome damage. J Leukoc Biol. 2010; 88:813–822. [PubMed: 20587739]
36. Swanson JA. Phorbol esters stimulate macropinocytosis and solute flow through macrophages. J Cell Sci. 1989; 94(Pt 1):135–142. [PubMed: 2613767]
37. Brandt S, Thorkildson P, Kozel TR. Monoclonal antibodies reactive with immunorecessive epitopes of glucuronoxylomannan, the major capsular polysaccharide of Cryptococcus neoformans. Clin Diagn Lab Immunol. 2003; 10:903–909. [PubMed: 12965925]
38. Kirkegaard T, Roth AG, Petersen NH, Mahalka AK, Olsen OD, Moilanen I, Zylicz A, Knudsen J, Sandhoff K, Arenz C, Kinnunen PK, Nylandsted J, Jaattela M. Hsp70 stabilizes lysosomes and reverts Niemann-Pick disease-associated lysosomal pathology. Nature. 2010; 463:549–553. [PubMed: 20111001]
39. Qiu Y, Davis MJ, Dayrit JK, Hadd Z, Meister DL, Osterholzer JJ, Williamson PR, Olszewski MA. Immune modulation mediated by cryptococcal laccase promotes pulmonary growth and brain dissemination of virulent Cryptococcus neoformans in mice. PLoS One. 2012; 7:e47853. [PubMed: 23110112]
40. Chen GH, McNamara DA, Hernandez Y, Huffnagle GB, Toews GB, Olszewski MA. Inheritance of immune polarization patterns is linked to resistance versus susceptibility to Cryptococcus neoformans in a mouse model. Infect Immun. 2008; 76:2379–2391. [PubMed: 18391002]
41. McCubbrey AL, Sonstein J, Ames TM, Freeman CM, Curtis JL. Glucocorticoids relieve collectin-driven suppression of apoptotic cell uptake in murine alveolar macrophages through downregulation of SIRPalpha. J Immunol. 2012; 189:112–119. [PubMed: 22615206]
42. Huotari J, Helenius A. Endosome maturation. EMBO J. 2011; 30:3481–3500. [PubMed: 21878991]
43. Osterholzer JJ, Milam JE, Chen GH, Toews GB, Huffnagle GB, Olszewski MA. Role of dendritic cells and alveolar macrophages in regulating early host defense against pulmonary infection with Cryptococcus neoformans. Infect Immun. 2009; 77:3749–3758. [PubMed: 19564388]
44. Vermaelen K, Pauwels R. Accurate and simple discrimination of mouse pulmonary dendritic cell and macrophage populations by flow cytometry: methodology and new insights. Cytometry A. 2004; 61:170–177. [PubMed: 15382026]

45. Nicola AM, Frases S, Casadevall A. Lipophilic dye staining of Cryptococcus neoformans extracellular vesicles and capsule. Eukaryot Cell. 2009; 8:1373–1380. [PubMed: 19465562]
46. Alanio A, Desnos-Ollivier M, Dromer F. Dynamics of Cryptococcus neoformans-macrophage interactions reveal that fungal background influences outcome during cryptococcal meningoencephalitis in humans. MBio. 2011:2.
47. Leenen PJ, Canono BP, Drevets DA, Voerman JS, Campbell PA. TNF-alpha and IFN-gamma stimulate a macrophage precursor cell line to kill Listeria monocytogenes in a nitric oxide-independent manner. J Immunol. 1994; 153:5141–5147. [PubMed: 7525724]
48. Bermudez LE, Young LS. Tumor necrosis factor, alone or in combination with IL-2, but not IFN-gamma, is associated with macrophage killing of Mycobacterium avium complex. J Immunol. 1988; 140:3006–3013. [PubMed: 2834450]
49. Alvarez M, Casadevall A. Phagosome extrusion and host-cell survival after Cryptococcus neoformans phagocytosis by macrophages. Curr Biol. 2006; 16:2161–2165. [PubMed: 17084702]
50. Ma H, Croudace JE, Lammas DA, May RC. Expulsion of live pathogenic yeast by macrophages. Curr Biol. 2006; 16:2156–2160. [PubMed: 17084701]
51. Stukes SA, Cohen HW, Casadevall A. Temporal kinetics and quantitative analysis of Cryptococcus neoformans nonlytic exocytosis. Infect Immun. 2014; 82:2059–2067. [PubMed: 24595144]
52. Hornung V, Bauernfeind F, Halle A, Samstad EO, Kono H, Rock KL, Fitzgerald KA, Latz E. Silica crystals and aluminum salts activate the NALP3 inflammasome through phagosomal destabilization. Nat Immunol. 2008; 9:847–856. [PubMed: 18604214]
53. Deepe GS Jr, Buesing WR. Deciphering the pathways of death of Histoplasma capsulatum-infected macrophages: implications for the immunopathogenesis of early infection. J Immunol. 2012; 188:334–344. [PubMed: 22102723]
54. Gross O, Poeck H, Bscheider M, Dostert C, Hannesschlager N, Endres S, Hartmann G, Tardivel A, Schweighoffer E, Tybulewicz V, Mocsai A, Tschopp J, Ruland J. Syk kinase signalling couples to the Nlrp3 inflammasome for anti-fungal host defence. Nature. 2009; 459:433–436. [PubMed: 19339971]
55. Hise AG, Tomalka J, Ganesan S, Patel K, Hall BA, Brown GD, Fitzgerald KA. An essential role for the NLRP3 inflammasome in host defense against the human fungal pathogen Candida albicans. Cell Host Microbe. 2009; 5:487–497. [PubMed: 19454352]
56. Said-Sadier N, Padilla E, Langsley G, Ojcius DM. Aspergillus fumigatus stimulates the NLRP3 inflammasome through a pathway requiring ROS production and the Syk tyrosine kinase. PLoS One. 2010; 5:e10008. [PubMed: 20368800]
57. Zang Y, Beard RL, Chandraratna RA, Kang JX. Evidence of a lysosomal pathway for apoptosis induced by the synthetic retinoid CD437 in human leukemia HL-60 cells. Cell Death Differ. 2001; 8:477–485. [PubMed: 11423908]
58. Cirman T, Oresic K, Mazovec GD, Turk V, Reed JC, Myers RM, Salvesen GS, Turk B. Selective disruption of lysosomes in HeLa cells triggers apoptosis mediated by cleavage of Bid by multiple papain-like lysosomal cathepsins. J Biol Chem. 2004; 279:3578–3587. [PubMed: 14581476]
59. Heinrich M, Neumeyer J, Jakob M, Hallas C, Tchikov V, Winoto-Morbach S, Wickel M, Schneider-Brachert W, Trauzold A, Hethke A, Schutze S. Cathepsin D links TNF-induced acid sphingomyelinase to Bid-mediated caspase-9 and -3 activation. Cell Death Differ. 2004; 11:550–563. [PubMed: 14739942]
60. Nagaraj NS, Vigneswaran N, Zacharias W. Cathepsin B mediates TRAIL-induced apoptosis in oral cancer cells. J Cancer Res Clin Oncol. 2006; 132:171–183. [PubMed: 16362335]
61. Sandes E, Lodillinsky C, Cwirenbaum R, Arguelles C, Casabe A, Eijan AM. Cathepsin B is involved in the apoptosis intrinsic pathway induced by Bacillus Calmette-Guerin in transitional cancer cell lines. Int J Mol Med. 2007; 20:823–828. [PubMed: 17982689]
62. Yacoub A, Park MA, Gupta P, Rahmani M, Zhang G, Hamed H, Hanna D, Sarkar D, Lebedeva IV, Emdad L, Sauane M, Vozhilla N, Spiegel S, Koumenis C, Graf M, Curiel DT, Grant S, Fisher PB, Dent P. Caspase-, cathepsin-, and PERK-dependent regulation of MDA-7/IL-24-induced cell killing in primary human glioma cells. Mol Cancer Ther. 2008; 7:297–313. [PubMed: 18281515]

63. Guicciardi ME, Bronk SF, Werneburg NW, Yin XM, Gores GJ. Bid is upstream of lysosome-mediated caspase 2 activation in tumor necrosis factor alpha-induced hepatocyte apoptosis. Gastroenterology. 2005; 129:269–284. [PubMed: 16012953]

64. Hishita T, Tada-Oikawa S, Tohyama K, Miura Y, Nishihara T, Tohyama Y, Yoshida Y, Uchiyama T, Kawanishi S. Caspase-3 activation by lysosomal enzymes in cytochrome c-independent apoptosis in myelodysplastic syndrome-derived cell line P39. Cancer Res. 2001; 61:2878–2884. [PubMed: 11306462]

65. Chen W, Li N, Chen T, Han Y, Li C, Wang Y, He W, Zhang L, Wan T, Cao X. The lysosome-associated apoptosis-inducing protein containing the pleckstrin homology (PH) and FYVE domains (LAPF), representative of a novel family of PH and FYVE domain-containing proteins, induces caspase-independent apoptosis via the lysosomal-mitochondrial pathway. J Biol Chem. 2005; 280:40985–40995. [PubMed: 16188880]

66. Boya P, Kroemer G. Lysosomal membrane permeabilization in cell death. Oncogene. 2008; 27:6434–6451. [PubMed: 18955971]

67. Kagedal K, Johansson AC, Johansson U, Heimlich G, Roberg K, Wang NS, Jurgensmeier JM, Ollinger K. Lysosomal membrane permeabilization during apoptosis--involvement of Bax? Int J Exp Pathol. 2005; 86:309–321. [PubMed: 16191103]

68. Feldstein AE, Werneburg NW, Canbay A, Guicciardi ME, Bronk SF, Rydzewski R, Burgart LJ, Gores GJ. Free fatty acids promote hepatic lipotoxicity by stimulating TNF-alpha expression via a lysosomal pathway. Hepatology. 2004; 40:185–194. [PubMed: 15239102]

69. Feldstein AE, Werneburg NW, Li Z, Bronk SF, Gores GJ. Bax inhibition protects against free fatty acid-induced lysosomal permeabilization. Am J Physiol Gastrointest Liver Physiol. 2006; 290:G1339–1346. [PubMed: 16484678]

70. Werneburg NW, Guicciardi ME, Bronk SF, Kaufmann SH, Gores GJ. Tumor necrosis factor-related apoptosis-inducing ligand activates a lysosomal pathway of apoptosis that is regulated by Bcl-2 proteins. J Biol Chem. 2007; 282:28960–28970. [PubMed: 17686764]

71. Skold M, Behar SM. Tuberculosis triggers a tissue-dependent program of differentiation and acquisition of effector functions by circulating monocytes. J Immunol. 2008; 181:6349–6360. [PubMed: 18941226]

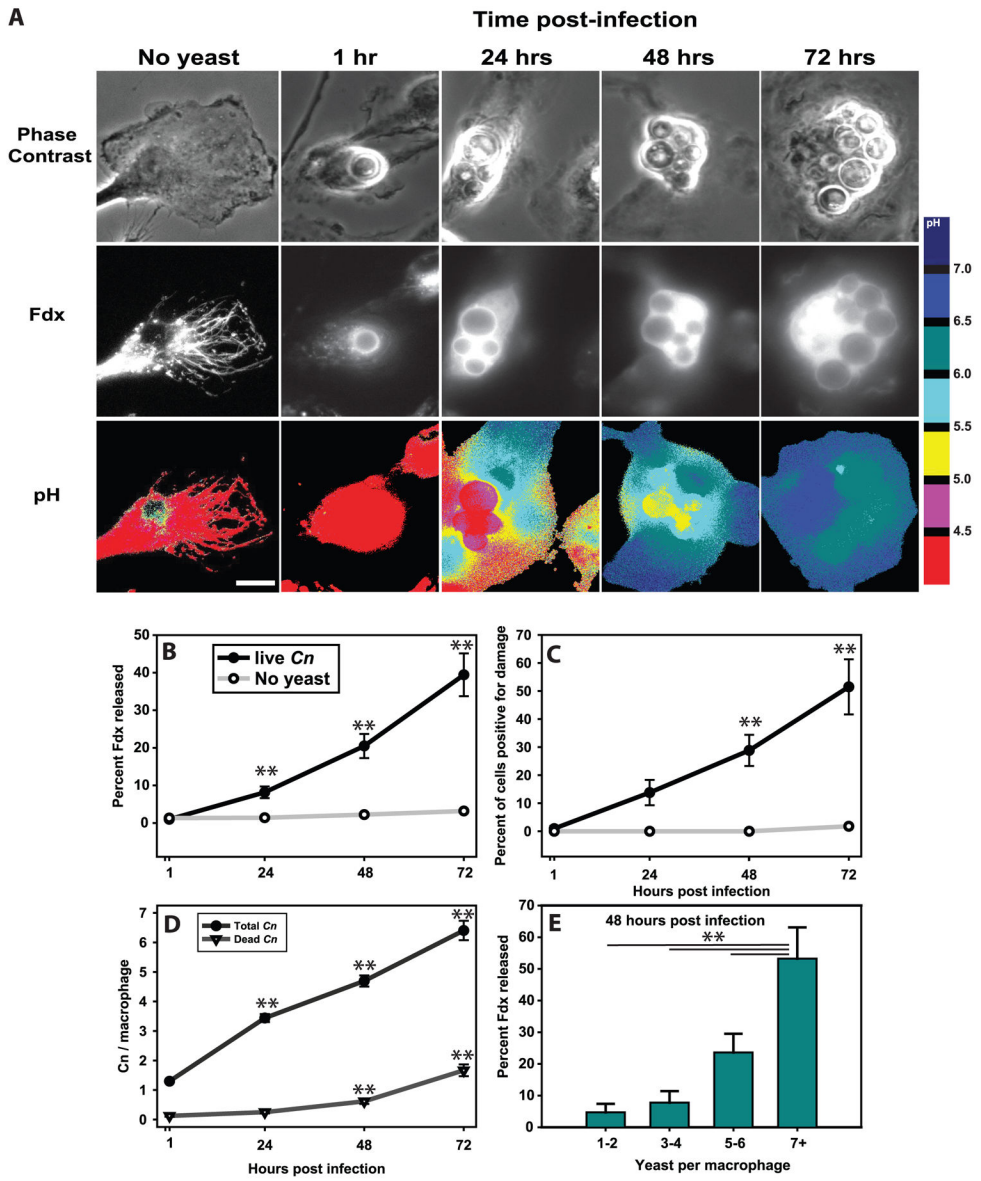

Figure 1. *Cryptococcus neoformans* induces lysosome damage that increases over time and with yeast replication

BMM lysosomes were loaded with Fdx during overnight incubation followed by 3 hours of chase in Fdx-free media. BMM were then infected with IgG-opsonized *Cn* strain H99. After one hour, excess yeast were rinsed away and cultures imaged immediately (1h post infection) or at 24, 48 and 72 hours post infection. (**A**) Representative images showing the phase contrast of macrophages and internalized *Cn* (top), Fdx distribution pattern within macrophages (middle) and pH maps, pseudo-colored such that each color represents a defined range of pH (bottom; pH color key is displayed to the right of the images). Scale bar in lower right represents 10 μm. (**B**) Average lysosome damage, quantified as the percent of Fdx released from the lysosome into the cytosol. (**C**) The data from B re-plotted as the percent of cells positive for lysosome damage (release greater than 10%). For B & C statistical comparisons are between infected and uninfected macrophages at each time point

and between indicated time points and live *Cn* containing cells at the 1 hr post infection time point. One symbol was displayed for each time point since both comparisons resulted in similar p values. (**D**) Mean number of total and dead *Cn* per analyzed macrophage. Statistical comparisons are between indicated time points and the 1 hr post infection time point. (**E**) Mean lysosome damage as a function of number of *Cn* per macrophage at 48 hours post-infection time point. Note that lysosome damage, the number of *Cn* and the number of killed *Cn* increased over the course of the experiment. Data are mean ± SEM and are combined from two independent experiments (total analyzed macrophages per time point n >100). For (B, D & E) ** indicates $p<0.005$, Student-Newman-Keuls.

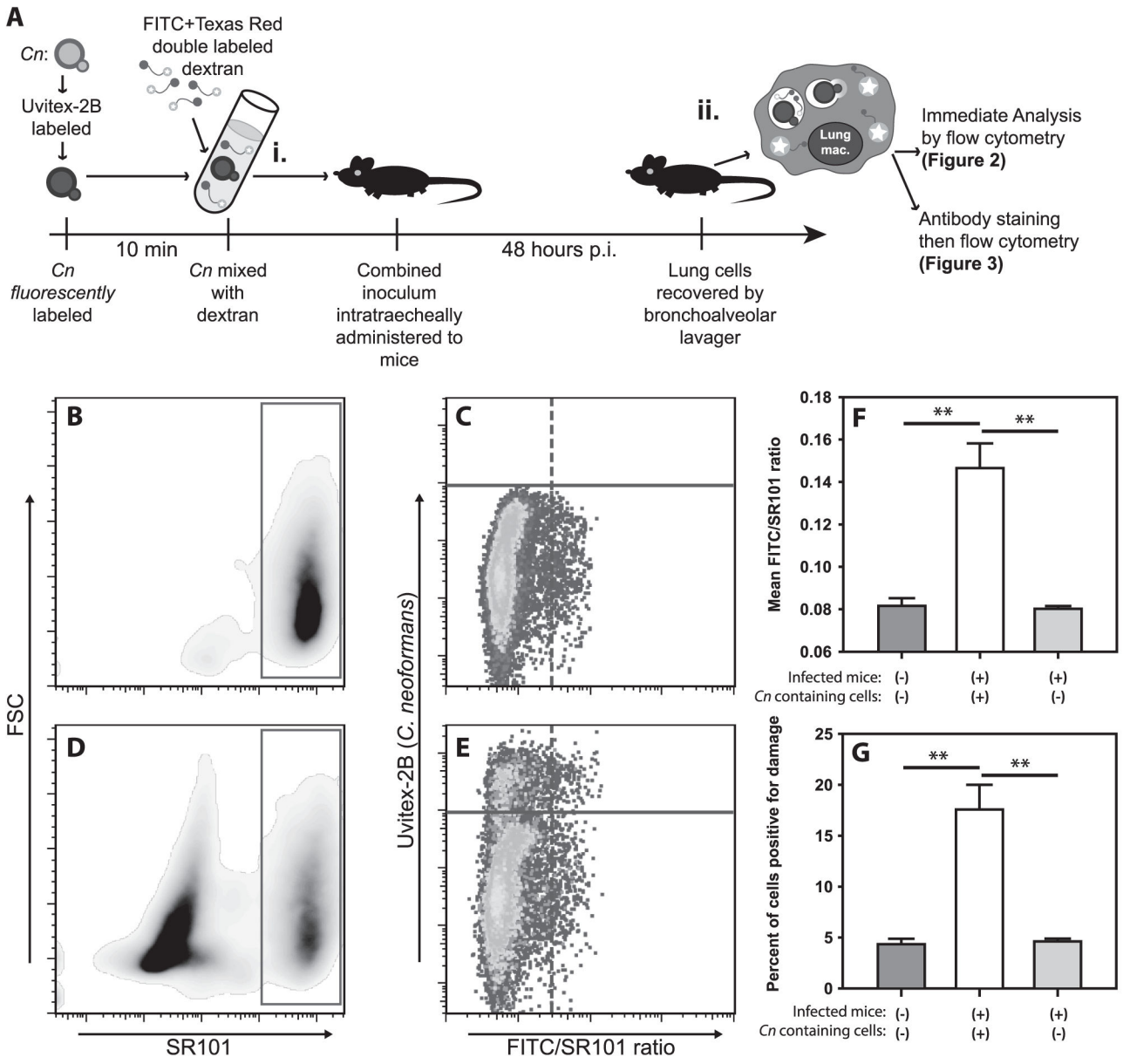

Figure 2. *C. neoformans* mediates damage during *in vivo* infection

(A) Schematic timeline of *in vivo* infection (i) and analysis strategy (ii). Briefly, mice received either F/SR101dx alone (B & **C**) or F/SR101dx and Uvitex-2B stained *Cn* (**D** & **E**) intratracheally and 48h later cells were harvested by BAL, stained with SYTOX red to exclude of dead cells and analyzed by flow cytometry. After gating on F/SR101dx+ live cells (**B** & **D, red box**), *Cn* containing cells (**C** & **E**; cells above the solid purple line) were distinguished from cells without *Cn* (**C** & **E**; cells below the solid purple line) on the basis of Uvitex-2B staining (Y-axis). The cells from the infected mice which contained *Cn* (E; above solid purple line) where then compared to uninfected cells from the same mice (E; below solid purple line) and those from uninfected mice (C) based on the ratio of FITC fluorescence to SR101 fluorescence (C & E; X-axis). Release of the F/SR101dx into the pH

neutral cytosol results in increased FITC signal with unchanged SR101 signal thus higher FITC/SR101 ratios indicated lysosome damage. Damage was quantitated as mean FITC/SR101 ratio (**F**) and the percentage of cells above a threshold for damage (**G**). Data are representative from one of two independent experiments with N = 5 mice for each condition in each experiment. F & G are mean ± SEM; ** indicates $p<0.005$, Student-Newman-Keuls.

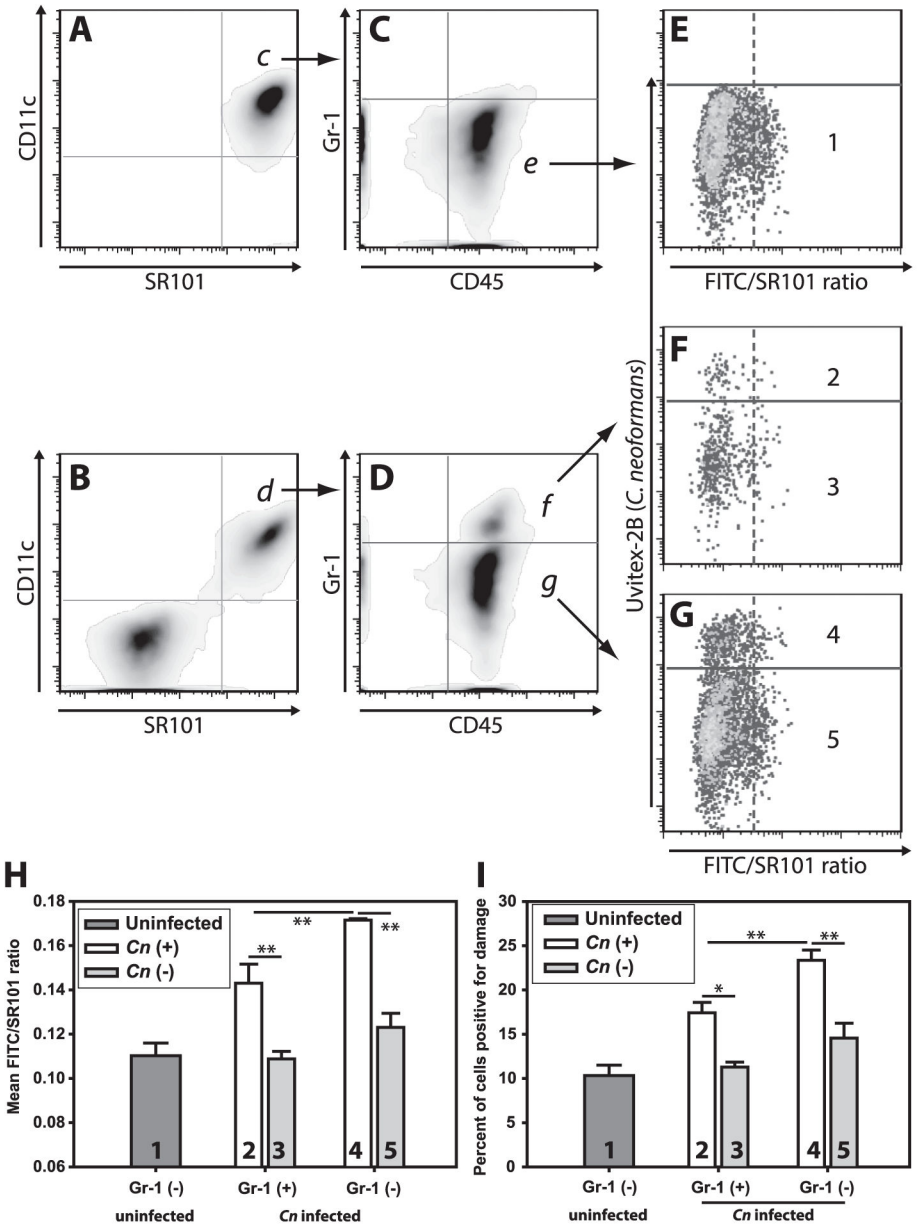

Figure 3. The vast majority of F/SR101dx-containing lung cells are alveolar macrophages

Mice were infected as in figure 2. Following recovery of lung airspace cells by BAL, cells were stained with fluorescently labeled antibodies against CD11c (a marker of monocytic myeloid cells), CD45 (a pan-leukocyte marker) and Gr-1 (a marker of recently recruited cells). Dead cells and debris were eliminated from analysis by live/dead staining. (**A–G**) are representative of the sequential gating scheme from F/SR101dx-administered uninfected mice (**A**, **C** & **E**) or from F/SR101dx-administered *Cn*-infected mice (**B**, **D**, **F** & **G**). Gated populations selected for further analysis are indicated with arrows and labeled corresponding to the panel where the indicated population is further analyzed. **A** & **B** display CD11c staining (Y-axis) and SR101 fluorescence (X-axis) from F/SR101dx. For **C** & **D**, SR101dx+ and CD11c+ double positive populations in panels A & B were further analyzed by plotting

Gr-1 (Y-axis) and CD45 (X-axis). Note that alveolar macrophages are known to be CD11c+ CD45+ and Gr-1^{dim} (indicated by populations “e” and “g”) while exudate macrophages are CD11c+ CD45+ and Gr-1+ (indicated by population “f”). For **E–G** sub-populations in C & D were analyzed for damage (FITC/SR101 ratio) on the X-axis and presence of cell-associated *Cn* (Uvitex-2B fluorescence) on the Y-axis. The various Gr-1+ or Gr-1^{dim} populations displayed in (C & D) were divided into *Cn*+ and *Cn*- populations as in Figure 6 and plotted in panels **H** & **I.** Populations indicated by the numbers **1–5** in E–G correspond to bars in panels H & I. As in Figure 2, damage was analyzed by plotting mean FITC/SR101 ratio (**H**) or the percent of cells positive for damage (**I**). Bars in H & I are means ± SEM with N=5 mice for each condition. * indicates $p<0.05$ and ** indicates $p<0.005$, Student-Newman-Keuls.

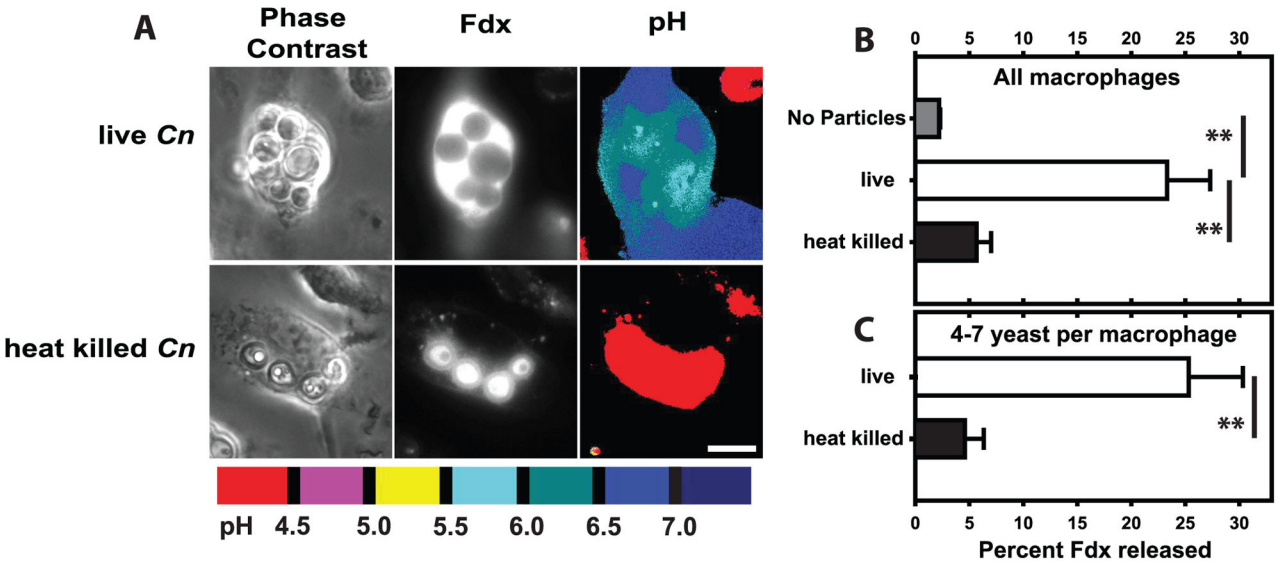

Figure 4. Induction of lysosome damage requires viable *C. neoformans.*

BMM lysosomes with Fdx were allowed to phagocytose IgG-opsonized live *Cn* or heat-killed *Cn* particles. At 48 hrs post-infection, lysosome damage and the number of yeast per BMM were determined. (**A**) Representative images of BMM containing live *Cn* or heat-killed *Cn*. Scale bar in lower right represents 10 μm. Lysosome damage for (**B**) all BMM and (**C**) the subset of BMM which contained 4–7 particles. Note that the killed *Cn* appear to be filled with Fdx whereas the live yeast exclude Fdx. Data are mean ± SEM, combined from two independent experiments (total analyzed macrophages per condition: B, $n > 90$; C, $n > 60$); ** indicates $p<0.005$; (B) Student-Newman-Keuls and (C) unpaired student t-test.

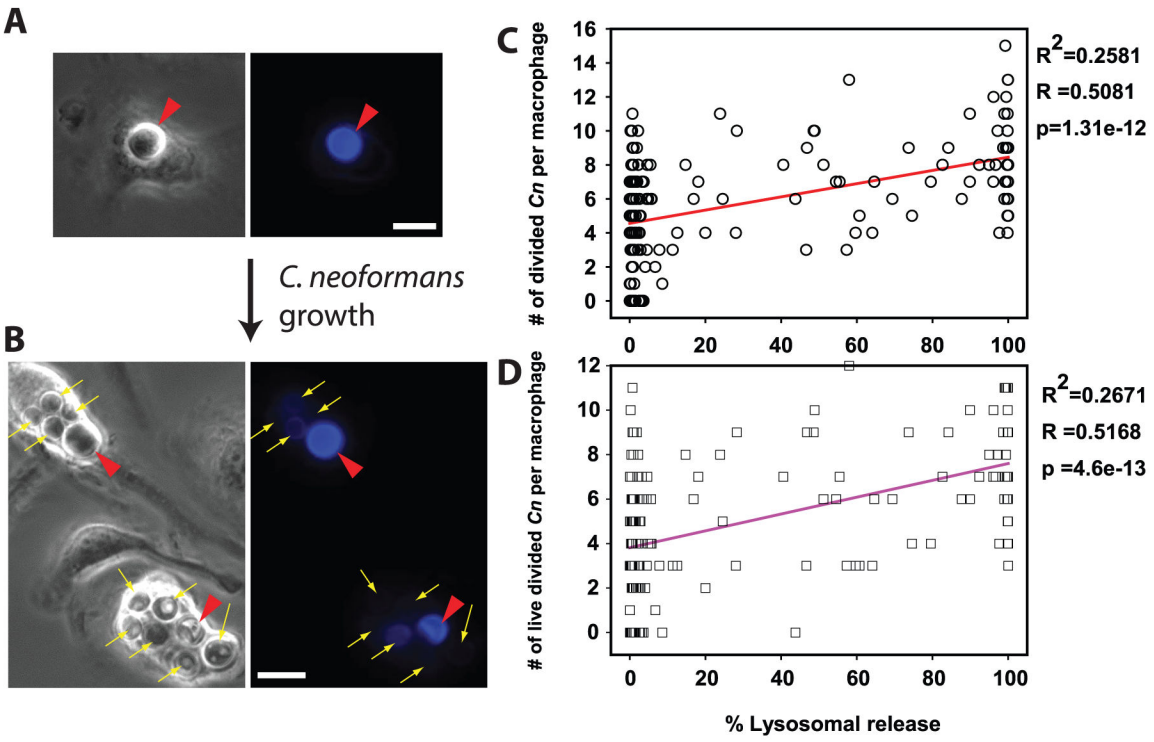

Figure 5. *C. neoformans*-mediated lysosome damage correlates with intracellular survival and replication of *C. neoformans*

Fdx-loaded BMM were infected with Uvitex-2B stained *Cn*, and were assayed immediately or after 48h for lysosome damage and for the number, viability status and Uvitex-2B fluorescence signal of intracellular yeast. **(A, B**) Representative BMM, at **(A)** Baseline, brightly fluorescent undivided Cn (red arrow heads); **(B)** 48 h, when replication of the yeast diluted Uvitex-2B, permitting distinction between *Cn* that had divided (thin yellow arrows) and *Cn* that had not divided (red arrow heads). In A and B scale bars in lower right represent 10 μm. (**C & D**) Relationship between lysosome damage (x-axis) to the number per BMM of: **(C)** divided *Cn*, (circles) or **(D)** viable, divided *Cn* (squares). Correlation parameters for the illustrated data sets are listed to the right of each graph. Lysosome damage correlated with intracellular survival and proliferation of *Cn*. Data are combined from five coverslips across two independent experiments, totaling N > 170 BMM.

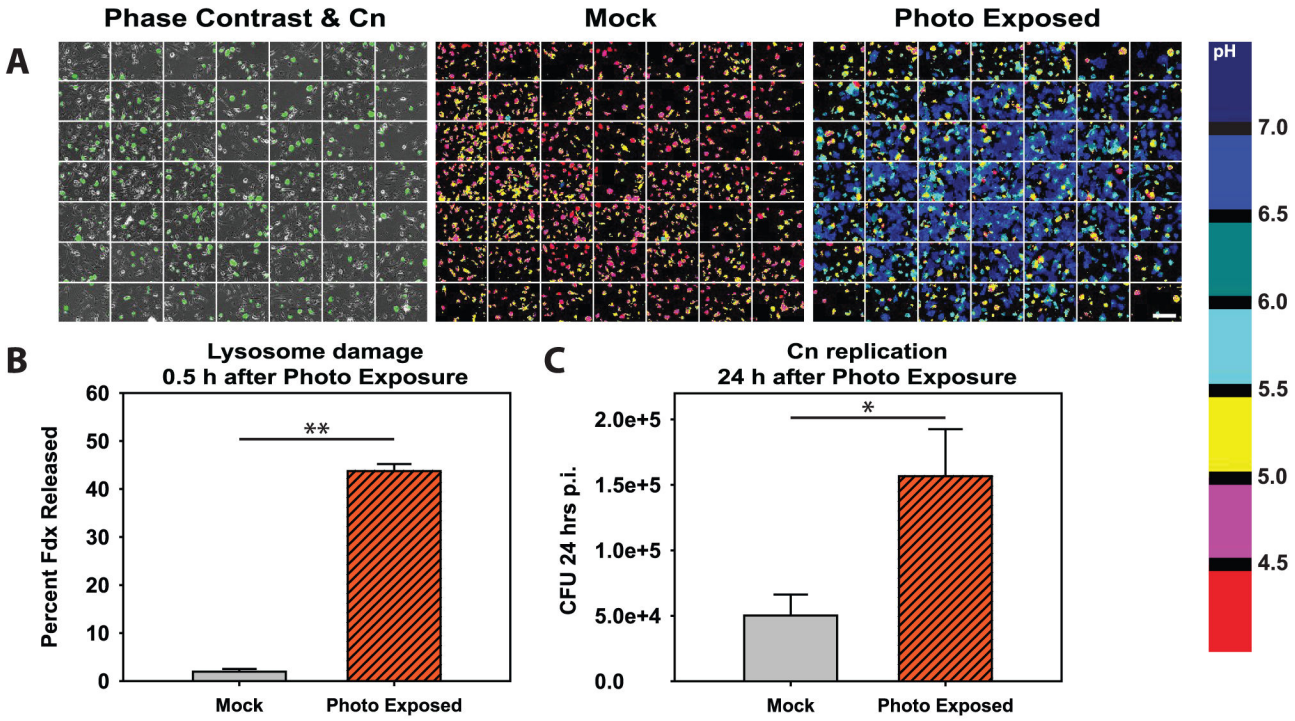

Figure 6. Photo exposure induced lysosome damage increases replication of *C. neoformans*

BMM were loaded with Fdx and Texas Red dextran then infected with Uvitex-2B-stained *Cn*. One group of coverslips was photo exposed using bright orange/red light ("Photo Exposed") while control coverslips were mock exposed ("Mock"). A grid array of images was then acquired of each coverslip using an automated acquisition sequence and the microscope motorized stage. **(A)** Representative images of coverslip imaging displaying 7 × 7 grids. Left panel displays phase contrast with Uvitex-2B staining overlayed in green to illustrate the presence of *Cn*. Middle and right panels display pH maps of a mock photo exposed coverslip (middle panel) and a photo exposed coverslip (right panel). The white scale bar in lower right of A represents 100 μm. (**B**) Average lysosome damage, quantified as the percent of Fdx released from the lysosome into the cytosol of the *Cn*-containing BMM. **(C)** Average CFU 24 post infection for coverslips photo exposed compared to mock exposed coverslips. In B & C data are combined from N > 5 coverslips combined from three independent experiments. * indicates $p<0.05$ and ** indicates $p<0.005$ student t test.

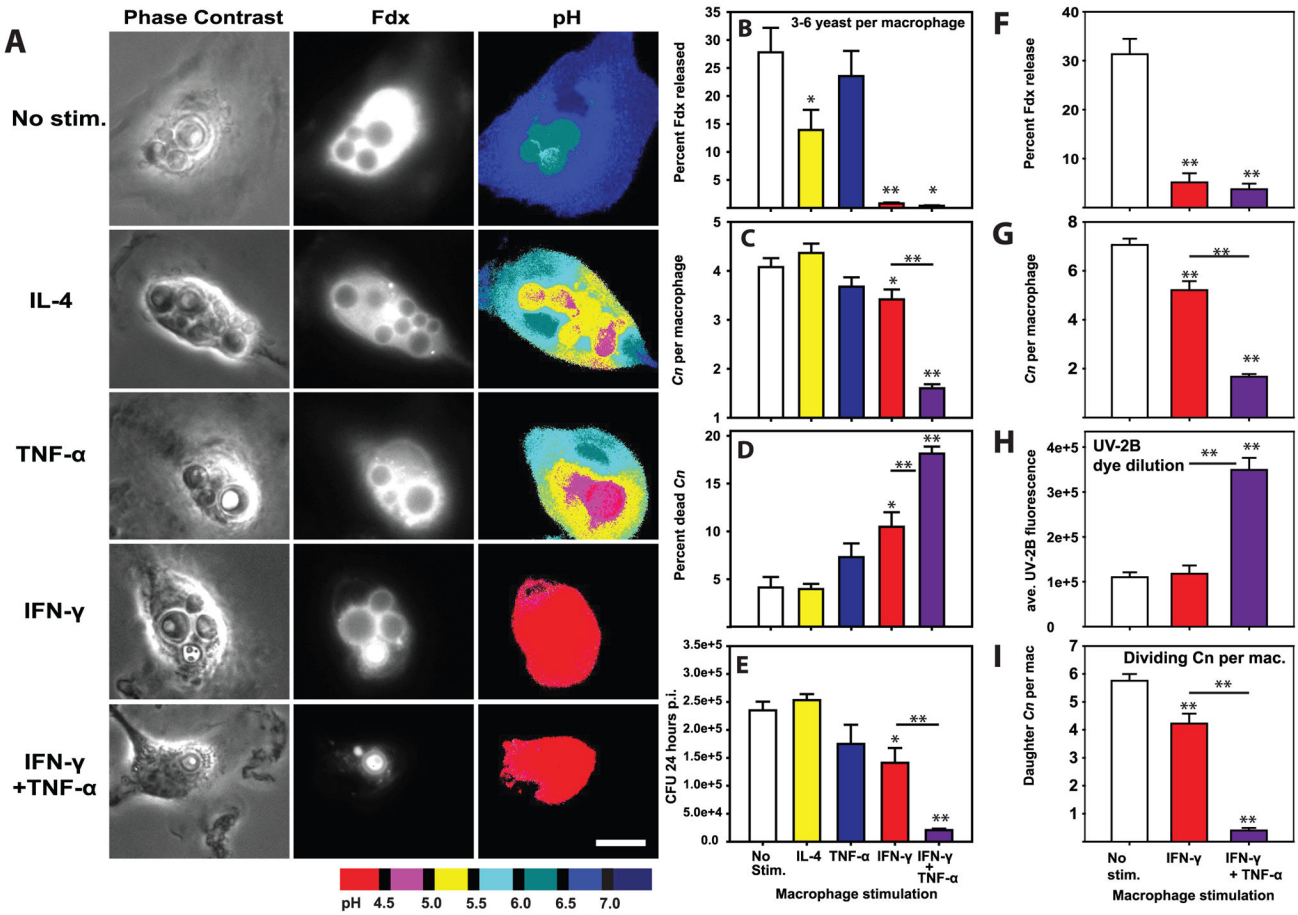

Figure 7. IFN-γ-stimulation of macrophages prevents *C. neoformans*-mediated lysosome damage and restricts *C. neoformans* replication

BMM were stimulated with 20 ng/mL IL-4, 20 ng/mL TNF-α, 100 ng/mL IFN-γ or 100 ng/mL IFN-γ plus 20 ng/mL TNF-α for 24h prior to infection with *Cn*. 24 hrs post-infection, *Cn*-containing BMM were analyzed for lysosome damage (**A** & **B**), the number of yeast per BMM (**C**) and the percent of dead *Cn* per macrophage (**D**). In A scale bar in lower right represents 10 μm. (**E**) In parallel experiments BMM were similarly stimulated and infected with *Cn*. The cultures were lysed 24 hours post infection and colony forming units enumerated. In B–D, N > 90 total analyzed macrophages in each condition combined from three independent experiments. In E, N = 6 wells combined from two independent experiments. A similar experiment was performed using BMM stimulated with 100 ng/mL IFN-γ or 100 ng/mL IFN-γ plus 20 ng/mL TNF-α for 24h prior to infection with uvitex-2B-stained *Cn*. 48 hours post infection, *Cn*-containing BMM were imaged and analyzed for lysosome damage levels (**F**), number of *Cn* per BMM (**G**), Intensity of Uvitex-2B staining in *Cn* (**H**) and the number of *Cn* per macrophage with dim Uvitex-2B staining indicating replicated *Cn* (**I**). In F–I, and are combined from 2 independent experiments. In N > 60 total analyzed macrophages in each condition. Bar graphs are mean ± SEM. Statistical comparisons not indicated by lines are to no-stimulation controls; comparisons between IFN-γ and IFN-γ + TNF-α conditions are indicated by lines. * indicates $p<0.05$ and ** indicates $p<0.005$ Student-Newman-Keuls.

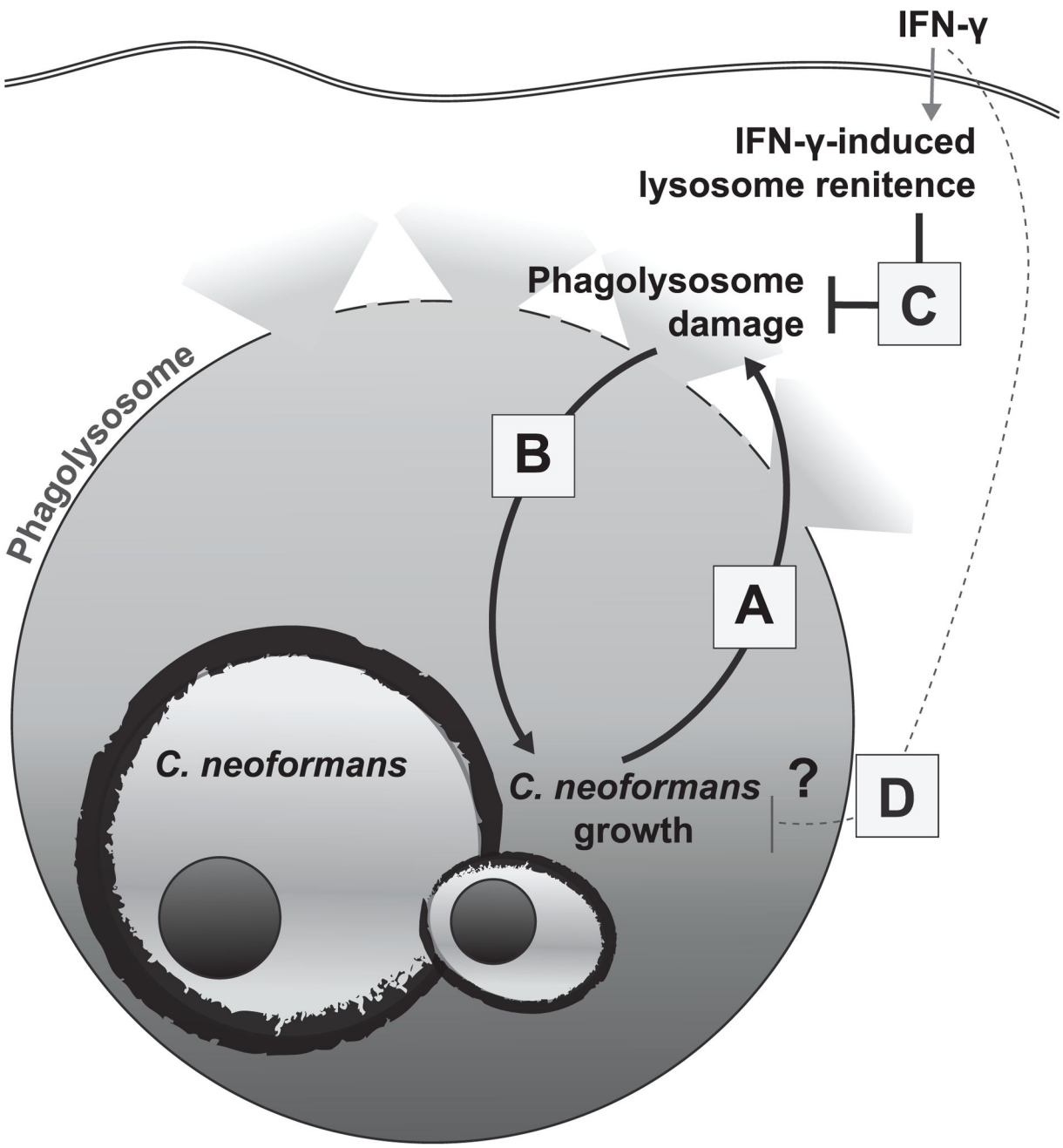

Figure 8. The role of *C. neoformans*-mediated lysosome damage as mediator of intracellular fungal virulence and its restriction for anti-fungal activity

The data presented above demonstrate that *Cn* induces progressive lysosome damage during the intracellular growth within macrophage **(A)** and that lysosome damage enhances *Cn* intracellular growth **(B)**. This vicious cycle is a crucial element of cryptococcal virulence. Stimulation of the macrophages with IFN-γ prevents *Cn*-induced phagolysosome damage **(C)** which is the proposed mechanism for restricted intracellular *Cn* growth and for fungicidal activity of macrophages.